JACS
JOURNAL OF THE AMERICAN CHEMICAL SOCIETY

Article

pubs.acs.org/JACS

Open Access on 05/23/2015

Intrinsic Conformational Plasticity of Native EmrE Provides a Pathway for Multidrug Resistance

Min-Kyu Cho,[†] Anindita Gayen,[†] James R. Banigan, Maureen Leninger, and Nathaniel J. Traaseth*

Department of Chemistry, New York University, New York, New York 10003, United States

Supporting Information

ABSTRACT: EmrE is a multidrug resistance efflux pump with specificity to a wide range of antibiotics and antiseptics. To obtain atomic-scale insight into the attributes of the native state that encodes the broad specificity, we used a hybrid of solution and solid-state NMR methods in lipid bilayers and bicelles. Our results indicate that the native EmrE dimer oscillates between inward and outward facing structural conformations at an exchange rate (k_{ex}) of ~300 s^{-1} at 37 °C (millisecond motions), which is ~50-fold faster relative to the tetraphenylphosphonium (TPP^+) substrate-bound form of the protein. These observables provide quantitative evidence that the rate-limiting step in the TPP^+ transport cycle is not the outward–inward conformational change in the absence of drug. In addition, using differential scanning calorimetry, we found that the width of the gel-to-liquid crystalline phase transition was 2 °C broader in the absence of the TPP^+ substrate versus its presence, which suggested that changes in transporter dynamics can impact the phase properties of the membrane. Interestingly, experiments with cross-linked EmrE showed that the millisecond inward-open to outward-open dynamics was not the culprit of the broadening. Instead, the calorimetry and NMR data supported the conclusion that faster time scale structural dynamics (nanosecond–microsecond) were the source and therefore impart the conformationally plastic character of native EmrE capable of binding structurally diverse substrates. These findings provide a clear example how differences in membrane protein transporter structural dynamics between drug-free and bound states can have a direct impact on the physical properties of the lipid bilayer in an allosteric fashion.

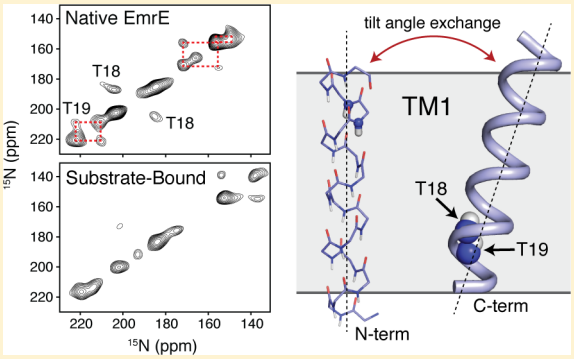

INTRODUCTION

Multidrug resistance (MDR) is a significant biomedical problem affecting the ability to treat bacterial infections and cancer.[1,2] Mechanisms resulting in antimicrobial resistance include modification to the target, enzymatic degradation of the drug, reduction of antibiotic permeability, and active drug efflux.[3] Molecular transporters residing in the cellular membrane give the broadest range of protection from toxic molecules.[4] These molecular machines are polytopic integral membrane proteins that bind a wide variety of drugs on the cytoplasmic side of cell, transport them across the lipid bilayer, and thus confer resistance to the host organism.[4] The most prevailing model used to explain ion-coupled secondary active transport involving efflux pumps is the alternating access model,[5] which involves oscillation between conformational states (i.e., protein dynamics) ultimately resulting in movement of the drug from the cytoplasmic to the periplasmic side of the membrane. The structural snapshots of MDR symporters and antiporters provided by crystallography have revealed a wealth of support for a dynamic energy landscape. Perhaps the best examples are those structures from the major facilitator superfamily, which include various structures in the inward-open, outward-open, and occluded configurations (reviewed in refs 6–8). Interestingly, the fold of these transporters contains the presence of inverted structural repeat domains[8,9] that resemble the smallest known efflux pumps of the small multidrug resistance (SMR) family.[10] This is one of the reasons the SMR family has emerged as an excellent model to study energy coupling and the broad recognition mechanism for biocides and antibiotics.[11]

The archetype SMR protein is EmrE, a four transmembrane (TM) domain transporter (SI Figure 1 in Supporting Information) that functions as a dimer, and has been suggested to be a *living fossil*.[12] Structural models determined using data from X-ray crystallography (3.8 Å) and cryoelectron microscopy (7.5 Å × 16 Å) have illuminated an antiparallel quaternary arrangement of the dimer.[13−15] This architecture has been supported with evidence from biophysical and biochemical methods including NMR spectroscopy,[16−18] single-molecule FRET,[18] and coexpression of single topology mutants.[19] Specifically, a combination of solution NMR and FRET experiments showed that the tetraphenylphosphonium (TPP^+)-bound form of EmrE undergoes a dynamic exchange whereby the monomeric subunits interconvert in a pseudo two-fold symmetry.[18] In this process, the transporter converts

Received: March 28, 2014
Published: May 23, 2014

   dx.doi.org/10.1021/ja503145x | J. Am. Chem. Soc. 2014, 136, 8072–8080

between inward-open and outward-open conformations at an exchange rate (k_{ex}) of ~9.6 s^{-1} at 45 °C.[18] These findings are also in agreement with the presence of multiple populations detected for Glu14 by magic-angle spinning NMR,[17] which is the key residue involved in energy coupling and substrate binding.[20,21] Additional evidence into the molecular basis of the transport mechanism was provided by oriented solid-state NMR experiments that sensitively probed the angular geometry of EmrE with respect to the lipid bilayer.[16] Our results showed two anisotropic chemical shifts for each residue, which provided atomic-scale insight into the asymmetric tilt angles of each monomer for both the native and TPP^+-bound states. Since only two anisotropic chemical shifts were observed for each residue, these findings were consistent with the angular asymmetry noted from the cryoelectron microscopy images[14] and the alternating access model.[5] In other words, the two populations corresponded to the monomers within either the inward-open or outward-open facing orientations relative to the cytoplasm, which constitutes an essential aspect of the transport cycle described by the alternating access model. However, the lack of additional populations does not eliminate the possibility of other intermediates such as an occluded conformation,[22] but it suggests that these states have a low occupancy in NMR samples lacking an asymmetric pH gradient. In fact, conformations other than inward-open or outward-open would be expected to have different tilt angles with respect to the lipid bilayer, which would have been sensitively probed by our PISEMA experiments.[16]

What are the properties of the native state that encode the ability to achieve broad molecular recognition for a wide range of structurally dissimilar biocides and antibiotics? While the cryoelectron microscopy images displayed no major differences between EmrE in the presence or absence of TPP^+,[14] the plasticity of the native state was inferred from differences between the substrate-bound forms.[23] These findings are consistent with those we reported from PISEMA spectroscopy,[16] where subtle conformational changes were observed within the transporter including those involved in an asymmetric bend in TM3. Thus, the ability to directly probe the dynamics of the native state is of paramount importance, as the conformational flexibility can be masked by static structural approaches or NMR chemical shifts that may be insensitive to the time scale of the motion. To provide direct insight, we utilized a hybrid of solution and solid-state NMR spectroscopy on native EmrE in lipid bilayers and bicelles. The portrait displayed by the NMR dynamics experiments illuminates the intrinsic conformational plasticity of native EmrE.

EXPERIMENTAL METHODS

Protein Production and Sample Preparation. [U-^{15}N], [U-^{13}C, ^{15}N, ^{2}H], and [ILV−$^{13}CH_3$, U−^{15}N, ^{2}H] labeled EmrE samples were expressed and purified as previously described with the addition of precursors at a concentration of 80 mg/L 2-ketobutyric acid-4-^{13}C,3,3-$^{2}H_2$ sodium salt hydrate and 2-keto-3-(methyl-$^{2}H_3$)-butyric acid-4-^{13}C,3-$^{2}H_1$ 1 h before induction for methyl labeling.[16] Selective labeling of [^{15}N-Thr] for oriented solid-state NMR was carried out as described previously.[16] [$^{13}C_\omega$,^{15}N-Leu] for magic-angle spinning solid-state NMR used 120 mg/L of isotopically labeled amino acid, 800 mg/L of natural abundance Val and Ile, and 300 mg/L of the other amino acids. Purified EmrE was reconstituted in 20% (w/v) DMPC/DHPC bicelles (q = 0.33) with perdeuteration of the lipid chains (14:0 PC D54 and 6:0 D22, Avanti Polar Lipids) as previously reported.[16] The final solution NMR samples contained ~0.5 mM EmrE in lipid bicelles with a buffer containing 20 mM Na_2HPO_4 (pH 6.9), 20 mM NaCl, 50 mM DTT, and 0.02% NaN_3. For probing the TPP^+-bound state, a final concentration of 2 mM was used. The preparation of [U-^{15}N] EmrE in DLPC/DHPC bicelle (q = 0.33) utilized the same procedure except that all the lipids were protonated and the ^{1}H/^{15}N TROSY-HSQC experiment was conducted on protonated [U-^{15}N] labeled protein. Ile, Val, and Leu methyl resonance assignments were obtained with single-site mutants prepared with the single-site mutagenesis kit from Agilent (Ile, I to L; Val, V to I; Leu, L to I).

EmrE Cross-Linking. The S107C mutant devoid of wild-type Cys residues (C39S, C41S, C95S) was grown and purified as previously described above.[16] The cross-linking reaction was performed using 190 μM S107C and 5 mM BMPS at pH 6.9 at 37 °C for 1 h. The reaction was quenched by addition of 100 mM DTT.

Solution NMR Experiments. Solution NMR spectra were acquired on Bruker 600, 800, and 900 MHz spectrometers with TCI cryoprobes or a QXI room temperature probe. For the temperature titrations, 2D ^{1}H/^{15}N TROSY-HSQC spectra and 2D ^{1}H/^{13}C HMQC spectra were acquired from 25 to 45 °C in 5 °C increments for both native and TPP^+-bound EmrE samples. The S107C cross-linked dimer (CL-EmrE) concentration was 0.23 mM, and the ^{1}H/^{15}N TROSY-HSQC spectra were acquired at 45 °C using a spectrometer with a ^{1}H frequency of 600 MHz and a room temperature QXI probe. The CL-EmrE experiment with TPP^+ had a final substrate concentration of 0.7 mM (3-fold excess dimer). Spectra were processed and analyzed with NMRPipe[24] and Sparky v3.113 (T.D. Goddard and D. G. Kneller, SPARKY 3, University of California, San Francisco).

Line Shape Fitting. Split peaks in 2D ^{1}H/^{15}N TROSY spectra and 2D ^{1}H/^{13}C TROSY spectra were analyzed using the NonlinearModelFit function in Mathematica (Wolfram Research). One-dimensional slices of the selected peaks (amide protons of W31 and G90; indole protons of W31 and W76; methyl protons of I5, I37, V34, and three unassigned methyl protons) were fitted to the equations below by varying the relaxation times (using T_{2A}, T_{2B}), exchange rate (k_{ex}), and chemical shift frequencies (ν):[25]

$$I(\nu) = -C_0(P[1 + \tau(p_B/T_{2A} + p_A/T_{2B})] + QR)/(P^2 + R^2) \quad (1)$$

where

$$P = \tau[1/(T_{2A}T_{2B}) - 4\pi^2\Delta\nu^2 + \pi^2\delta\nu^2] + p_A/T_{2A} + p_B/T_{2B}$$

$$Q = \tau[2\pi\Delta\nu - \pi\delta\nu(p_A - p_B)]$$

$$R = 2\pi\Delta\nu[1 + \tau(1/T_{2A} + 1/T_{2B})] + \pi\delta\nu\tau(1/T_{2B} - 1/T_{2A}) + \pi\delta\nu(p_A - p_B)$$

$$\delta\nu = \nu_A - \nu_B$$

$$\Delta\nu = (\nu_A + \nu_B)/2 - \nu$$

$$\tau = p_A/k_B = p_B/k_A = 1/k_{ex}$$

The two populations have subscripts A and B; p_A and p_B are the fractional populations ($p_A + p_B = 1$, $p_A = p_B = 0.5$ for EmrE); T_{2A} and T_{2B} are the transverse spin relaxation times; k_A and k_B are rate constants from each state to the other; ν_A and ν_B are the resonance frequencies for the two states. Note that for EmrE, $k_A + k_B = 2k = k_{ex}$.

Solid-State NMR Experiments. Solid-state NMR experiments were carried out on a DirectDrive2 Agilent spectrometer (14.1 T, ^{1}H frequency of 600 MHz). MAS was carried out at a spinning frequency of 12.5 kHz and utilized a sample of 4 mg of [$^{13}C_\omega$,^{15}N-Leu] EmrE reconstituted into DMPC lipids at a lipid/protein ratio of 85/1 (mol/mol).[26] The sample was packed into a 3.2 mm rotor with sample spacers to prevent dehydration. The ^{1}H $\pi/2$ pulse was 2.5 μs, and ^{1}H/^{13}C cross-polarization used a 0.25 ms contact time, a Hartmann−Hahn match at ~45 kHz on the ^{13}C channel, and an adiabatic tangent ramp on ^{1}H.[27] Two-dimensional ^{13}C/^{13}C PDSD experiments[28] were carried out on native EmrE at temperatures of 9 and −22 °C as

dx.doi.org/10.1021/ja503145x | J. Am. Chem. Soc. 2014, 136, 8072−8080

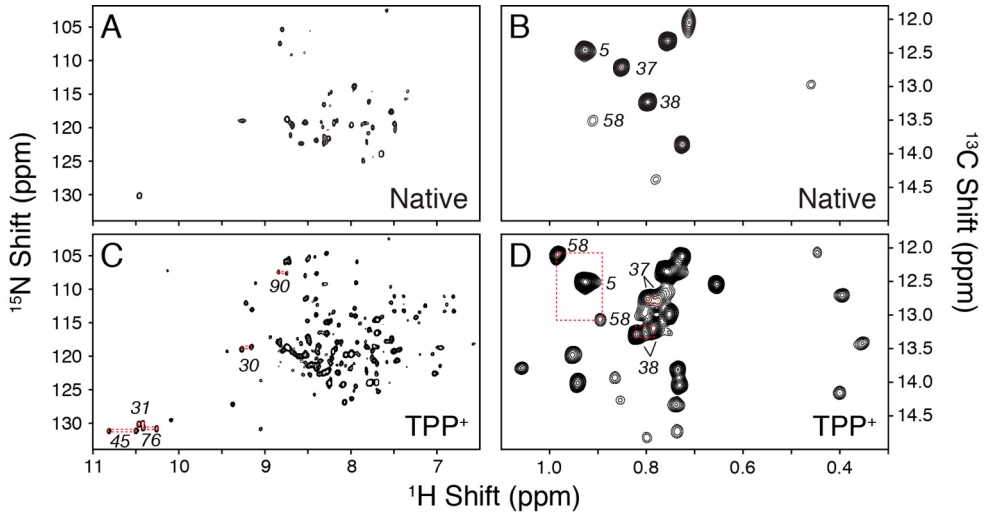

Figure 1. Solution NMR spectra of EmrE in the native and substrate-bound forms at 45 °C. $^{1}H/^{15}N$ TROSY-HSQC spectra for native and TPP^{+}-bound EmrE are shown in panels A and C, respectively. The Ile methyl groups were imaged using $^{1}H/^{13}C$ HMQC experiments in the native (B) and TPP^{+}-bound states (D).

determined by a methanol calibration.[29] For the experiments at 9 °C, a series of 2D spectra were acquired with mixing times of 0.1, 0.3, 0.5, 0.8, and 1.5 s in order to fit the exchange rate. The direct and indirect ^{13}C dimensions (acquisition or evolution time) were 100 kHz (25 ms) and 1562.5 Hz (11.5 ms), respectively. ^{1}H decoupling in the direct and indirect dimensions was carried out using TPPM at a field strength of 100 kHz.[30] The longitudinal relaxation rate (R_1) was measured for each diagonal peak in the PDSD spectra. The exchange rate was found by globally fitting the cross-peak intensities to the equation below (x is a scaling factor):[31]

$$I_{AB}(t) = x(1 - e^{-k_{ex}t})e^{-R_1 t} \quad (2)$$

^{13}C chemical shifts were referenced to 40.48 ppm using the CH_2 peak of adamantane.[32]

Oriented solid-state NMR experiments were carried out using [U-^{15}N] and [^{15}N-Thr] labeled samples of EmrE at a concentration of ~1.5 mM in 25% (w/v) DMPC/DHPC bicelles (q = 3.2) at 37 °C. The final buffer contained 20 mM HEPES (pH 6.9), 20 mM NaCl, 50 mM DTT, and 0.02% NaN_3. The sample was *flipped* with the addition of $YbCl_3$ to a final concentration of 3 mM. The experiments for TPP^{+}-bound EmrE used a 6-fold excess concentration relative to the dimer. The $^{15}N/^{15}N$ 2D PDSD experiment on [^{15}N-Thr] used $^{1}H/^{15}N$ cross-polarization for 0.75 ms and an effective field match of 50 kHz with ^{1}H SPINAL-64 decoupling[33] at 50 kHz. The direct and indirect ^{15}N dimensions (acquisition or evolution time) were 100 kHz (5 ms) and 10 kHz (1.4 ms), respectively. A recycle delay of 3 s with 3072 scans was used to give a total experimental time of 72 h. The ^{15}N mixing time, which served as a ZZ-exchange experiment[34] was set to 75 ms.

The PUREX experiment on [U-^{15}N] EmrE was used to quantify the exchange rate in magnetically aligned bicelles.[35] The modulation time τ was set to 250 μs to collect the frequency-modulated and reference spectra. The mixing time was varied from 0.125 to 750 ms for TPP^{+}-bound EmrE and 0.125 to 100 ms for the native state; experiments were repeated at 0.25 and 10 ms for error estimation. The frequency-modulated and reference spectra were acquired with 1536 and 768 scans, respectively. In order to account for relaxation and derive the contribution of conformational exchange, a difference spectrum was obtained by subtracting the frequency-modulated spectrum from that of the reference. Due to the small signal remaining in the difference spectra for short mixing times, we multiplied the frequency-modulated spectra by 1.06 for native and TPP^{+}-bound data sets prior to the subtraction. The resulting 1D difference spectra were integrated and reported without any additional normalization. These integrated intensities were fit to the equation below (x is scaling factor, and k_{ex} is exchange rate):[36]

$$I_{AB}(t) = x(1 - e^{-k_{ex}t}) \quad (3)$$

Note that the experiments for native and TPP^{+}-bound EmrE were carried out on the same sample, and therefore the intensities were directly comparable between the TPP^{+}-free and -bound forms. In addition, a second PUREX data set was obtained with a separately prepared [U-^{15}N] labeled sample (see Supporting Information). The reported exchange rates in SI Table I reflect a globally fit k_{ex} value from both samples. All ^{15}N spectra were referenced to 41.5 ppm with the use of $^{15}NH_4Cl$(s).

Differential Scanning Calorimetry. Differential scanning calorimetry (DSC) experiments were carried out on a nanoDSC (model 6300) from TA Instruments. For the experiments on the native and TPP^{+}-bound states of EmrE, a DMPC/dimer ratio of 200:1 (mol/mol) was used. The temperature range was 5–45 °C using a scanning rate of 0.5 °C/min for EmrE samples and 1.0 °C/min for lipid controls with an equilibration time of 600 s at a constant pressure of 3 atm. The melting temperature (T_m) and enthalpy of the main phase transition were determined using NanoAnalyze software v2.4.1 (TA Instruments). The main phase transition peaks were fit using the built-in *twostatescaled* model in NanoAnalyze. The transition half-height temperatures (i.e., full width at half-height, $\Delta T_{1/2}$) are given in SI Table II.

RESULTS AND DISCUSSION

Native EmrE Dynamics in Isotropic Bicelles Using Solution NMR. In order to carry out high-resolution solution NMR experiments, EmrE was isotopically enriched with ^{15}N at all residues and $^{13}CH_3$ at Ile $C_{\delta 1}$, Val $C_{\gamma 1/2}$, and Leu $C_{\delta 1/2}$ methyl groups in a perdeuterated background. The transporter was reconstituted into DMPC/DHPC isotropic bicelles (q = 0.33), which preserves TPP^{+} binding and corresponds to correctly folded protein.[16,18] In agreement with previous solution NMR findings carried out in the presence of TPP^{+},[18] we obtained a well-dispersed $^{1}H/^{15}N$ TROSY-HSQC spectrum at 45 °C (Figure 1C) that is consistent with peak doubling and an overall antiparallel configuration of the EmrE dimer. The ^{13}C methyl labeling also enabled us to probe side chain chemical shifts in addition to those of the amide backbone. Consistent with the $^{1}H/^{15}N$ TROSY spectrum, we observed peak doubling at the methyl groups in a $^{1}H/^{13}C$ HMQC experiment (i.e., methyl-TROSY[37]) that was indicative of monomer asymmetry at sites located in each of the four TM

dx.doi.org/10.1021/ja503145x | J. Am. Chem. Soc. 2014, 136, 8072–8080

domain helices (Figure 1D). However, unlike the results in the presence of TPP$^+$, we found that the native spectra at 45 °C for both the amide and methyl sites were relatively unresolved and devoid of several resonances (Figure 1A,B). For example, the Ile methyl peaks observed in the spectrum had only one broader apparent population (Figure 1B). The broadness of the peaks was characteristic of conformational heterogeneity and/or intermediate time scale motion and suggested *at first glance* that solution NMR studies would be incompatible with detailed structural and dynamic studies of the native form of EmrE.

To further investigate the underlying reasons for the spectral differences, we lowered the temperature from 45 to 20 °C in 5 °C increments with subsequent ^{1}H/^{15}N TROSY-HSQC and ^{1}H/^{13}C HMQC experiments acquired to probe both the backbone and side chain chemical shifts, respectively. In contrast to the spectra for TPP$^+$-bound EmrE, temperature had a pronounced effect on the number of peaks observed in ^{1}H/^{15}N TROSY-HSQC spectra for native EmrE (Figure 2).

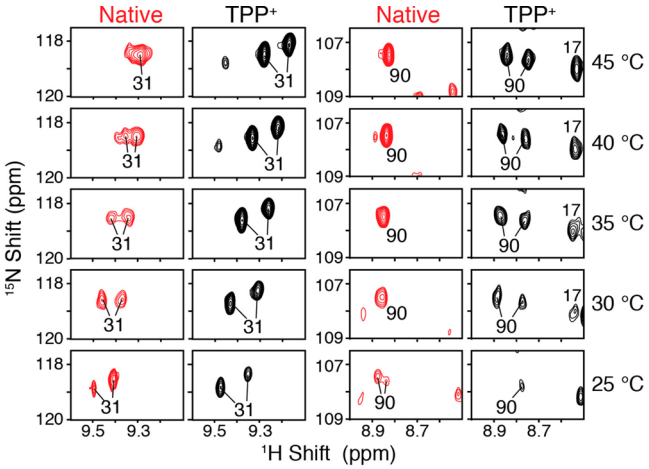

Figure 2. Native EmrE shows temperature-dependent splitting at backbone amide residues. Trp31 and Gly90 amide backbone cross-peaks of EmrE from ^{1}H/^{15}N TROSY-HSQC NMR spectra acquired at several temperatures indicated within the figure. Red spectra correspond to native EmrE, while the black spectra are for the TPP$^+$-bound form of the protein.

Specifically, we observed peak splitting for several sites with the most noticeable changes occurring to the side chain indoles of W31, W45, and W76 (Figure 3A). In fact, the indole peak positions for native EmrE at temperatures above 35 °C were located at an intermediate position between the two extremes observed for the TPP$^+$-bound transporter, which supported the presence of a single exchange event. Importantly, the chemical shifts at 25 °C were in agreement with those of TPP$^+$-bound EmrE (Figures 2 and 3 and SI Figure 2). One potential concern of our temperature-dependent experiments was the fact that the long-chain lipid in the bicelles (DMPC) had a phase transition temperature (T_m) of ∼23 °C. To address this, we repeated the temperature-dependent spectra using native EmrE in DLPC containing bicelles and observed similar peak splitting at 25 °C as those of the DMPC bicelles (SI Figure 3).

In addition to the splitting observed at the backbone amides, we also observed the appearance of extra peaks for Ile, Leu, and Val methyl resonances at lower temperatures including Ile5, Val34, Ile37, and Leu70 in the ^{1}H/^{13}C HMQC spectra (SI Figures 4 and 5). These observations indicated that the backbone and side chains were similarly affected by the conformational exchange and were distributed throughout the transporter. To quantify the conformational dynamics (k_{ex}) for native EmrE, we carried out line shape fitting in a global fashion for all resolved peaks displaying temperature-dependent splitting in the spectra using a two-state exchange model (Figure 3B and SI Figure 6).[25] The fitted values are shown in SI Table I and Figure 3B with k_{ex} ranging from ∼500 s^{-1} at 45 °C to 40 s^{-1} at 25 °C. Interestingly, the exchange rate for native EmrE is ∼50-fold larger than that reported for the TPP$^+$-bound form of the transporter at 45 °C.[18]

Validation of Exchange in Lipid Bilayers and Aligned Bicelles Using Solid-State NMR. To further validate the dynamics experiments obtained in isotropic bicelles, we carried out solid-state NMR spectroscopy in DMPC lipid bilayers and magnetically aligned bicelles (q = 3.2). The beauty of the oriented solid-state NMR approach is the ability to directly probe membrane protein structure with respect to the lipid bilayer surface.[38−45] Using PISEMA spectroscopy,[46−48] we previously found that the native and TPP$^+$-bound forms of EmrE have asymmetric monomer orientations relative to the lipid bilayer normal with substrate-induced structural changes occurring throughout the protein.[16] Unlike the solution NMR data at 37 °C (broadening characteristic of intermediate exchange), the PISEMA spectrum showed two clearly resolved populations. *Does EmrE experience the same conformational exchange in the isotropic and magnetically aligned bicelle samples?*

To directly quantify the rate of exchange between the two populations, we carried out dynamics experiments in the magnetically aligned bicelle samples. We used a [U-^{15}N] sample of EmrE and applied the pure exchange (PUREX) method,[35] which is an experiment to cancel diagonal peaks and only observe cross-peaks arising from conformational or magnetization exchange. While the variable mixing element in the PUREX method corresponds to proton-driven spin diffusion (PDSD),[28] in our application, magnetization exchange is not possible given the weak dipolar couplings between nearest ^{15}N neighbors.[49] Therefore, the PUREX serves as a type of ZZ-exchange experiment.[34] We carried out this method by recording a series of 1D spectra over a wide range of mixing times (SI Figure 7) with the integrated intensities shown in Figure 4 for EmrE in the absence and presence of TPP$^+$. From the PUREX data, we calculated exchange rates of 350 and 6.5 s^{-1} for the native and substrate-bound states at 37 °C, respectively, which were in excellent agreement with our solution NMR data and validated the conclusion that the native protein has an apparent ∼50-fold faster inward−outward conformational exchange than the TPP$^+$-bound form. In addition, the integrated intensities in Figure 4 leveled off to the same value at long mixing times and is strong support that the number of residues involved in the exchange for the native and TPP$^+$-bound states are the same, which reflects a global process felt throughout the transporter. These dynamics data also explain why we observed two populations for the native form in slow chemical exchange by PISEMA spectroscopy, which stems from the ∼25-fold larger chemical shift difference ($\Delta\omega$) between the monomer populations for the aligned bicelle samples ($k_{ex} < \Delta\omega$) versus those observed by solution NMR ($k_{ex} \sim \Delta\omega$).[16]

In order to provide further validation for individual sites within EmrE, we prepared a selectively labeled [^{15}N-Thr] sample that has residues located within the TM domains of the protein. The 2D ^{15}N/^{15}N PDSD spectra acquired with [^{15}N-Thr] EmrE used a mixing time of 75 ms and showed the

dx.doi.org/10.1021/ja503145x | J. Am. Chem. Soc. 2014, 136, 8072−8080

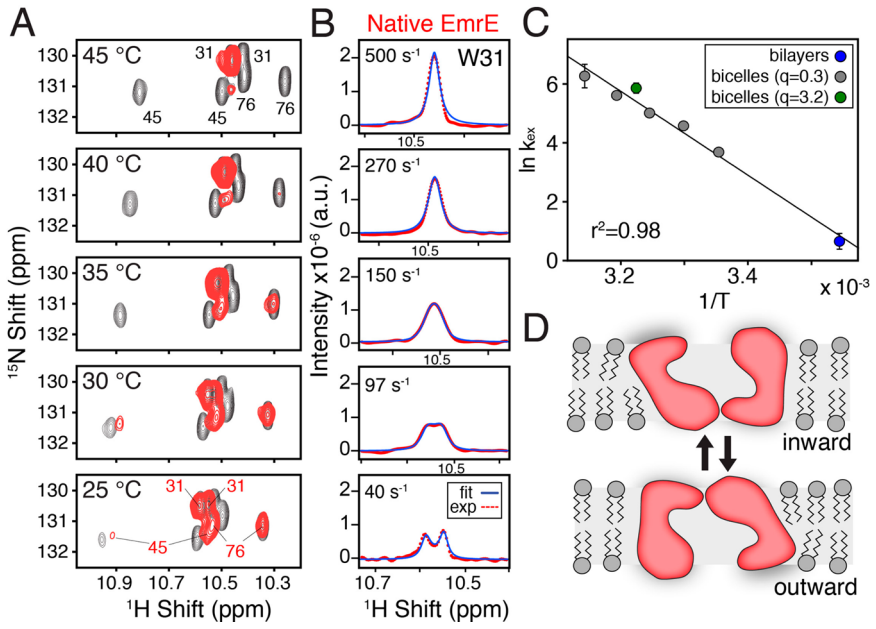

Figure 3. Temperature-dependent NMR spectra and activation energy. (A) $^{1}H/^{15}N$ TROSY-HSQC spectra in DMPC/DHPC isotropic bicelles that highlight the Trp indole region of native (red) and TPP^{+}-bound EmrE (black). (B) One-dimensional experimental (red) and fitted line shapes (blue) for the indole Trp31 residue of native EmrE. The fitted line shapes were obtained from a global fitting procedure that included all resolved residues displaying temperature-dependent peak splitting. (C) Arrhenius plot constructed from all exchange rates reported in SI Table I (i.e., solution NMR, oriented solid-state NMR, and MAS). (D) Model of the inward-open to outward-open conformational change that gives rise to two populations observed in EmrE.

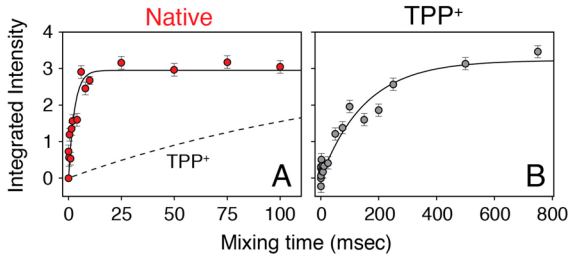

Figure 4. Conformational exchange rate measured in oriented lipid bicelles. Integrals from 1D ^{15}N PUREX[35] on [U-^{15}N] EmrE in DMPC/DHPC magnetically aligned bicelles at 37 °C in the (A) native and (B) TPP^{+}-bound states. Note the difference in the *x*-axis between panels A and B. To illustrate this difference, the best fit to the TPP^{+} data is shown in a dashed line with the native protein results in panel A. The k_{ex} values were obtained by globally fitting PUREX results from two separately prepared samples (SI Figure 11) that gave best fits of 350 ± 60 and 6.5 ± 0.9 s^{-1} for the native and TPP^{+}-bound forms, respectively.

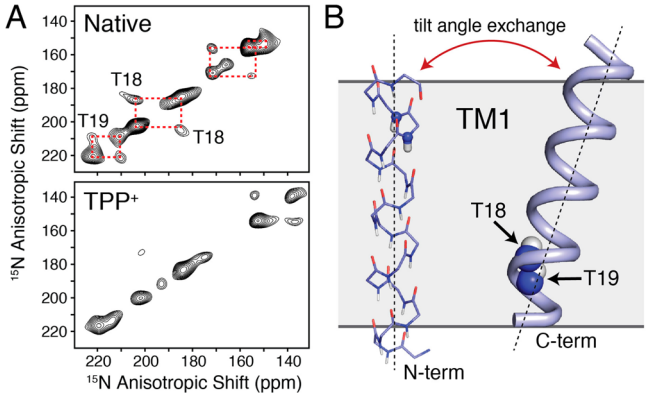

Figure 5. Tilt angle exchange observed by oriented solid-state NMR. (A) $^{15}N/^{15}N$ PDSD experiments for native and TPP^{+}-bound EmrE labeled with [^{15}N-Thr] at a mixing time of 75 ms and a temperature of 37 °C. The cross-peaks at 155 and 170 ppm have been tentatively assigned to Thr50, which is based on our Val34 assignment in TM2,[16] known helical wheel geometries, and comparison with back-calculated PISEMA spectra from EmrE structural models. (B) TM1 of EmrE from *2I68*[50] highlighting Thr18 and Thr19 and the corresponding changes in tilt angle with respect to the lipid bicelle that accompany the conformational exchange between the two populations. The tilt angles for the two TM1 helices of EmrE were calculated to be 16° and 33° relative to the membrane normal (SI Figure 8).

presence of intense cross-peaks for native EmrE that were absent or significantly reduced after addition of TPP^{+} (Figure 5). Specifically, Thr18 and Thr19 located within TM1 gave intense cross-peaks that were largely absent in the TPP^{+}-bound spectrum. Due to the helical geometry, Thr18 is located on the same face of the helix as the conserved Glu14 and positioned toward the binding pocket in the EmrE structural models.[13,15,50] These PDSD data are consistent with the PUREX results and further complement our solution NMR findings.

In addition to the dynamics data, the position of the chemical shifts of Thr18 and Thr19 coupled with our previous Val15 and Met21 assignments[16] enabled a calculation of the tilt angles for the two TM1 helices within the asymmetric dimer (SI Figure 8). Our calculation indicated that the two TM1 helices oscillate between tilt angles of ~16° and ~33° relative to the lipid bilayer normal, consistent with our previous findings that each monomer is asymmetrically oriented with respect to the membrane surface.[16] This whole-body conformational exchange orients EmrE between outward-open and inward-open configurations, which positions Glu14 ready for proton binding and release, respectively.

Finally, to obtain a k_{ex} value over a larger temperature range, we carried out exchange experiments of native EmrE labeled

dx.doi.org/10.1021/ja503145x | J. Am. Chem. Soc. 2014, 136, 8072−8080

with [$^{13}C_{\alpha}$,^{15}N-Leu] in DMPC lipid bilayers using magic-angle spinning (MAS). The selective labeling was used to improve the spectral resolution by removing $^{13}C-^{13}C$ J-couplings that lead to broadening in fully ^{13}C labeled samples.[26,51,52] Note that the solution NMR experiments could not be carried out at lower temperatures due to the slow reorientation and resulting loss of signal intensity. Similar to our results in isotropic and aligned bicelles, we observed two populations for Leu83 and Leu104 in slow chemical exchange at 9 °C using a $^{13}C/^{13}C$ PDSD experiment (Figure 6). The cross-peak intensities were

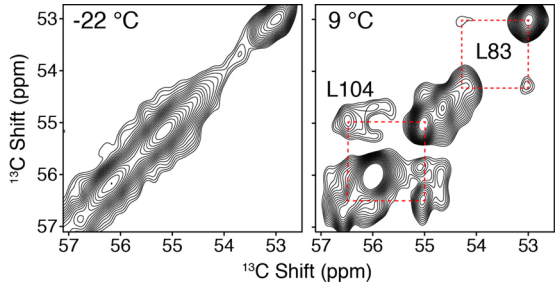

Figure 6. MAS exchange experiments in DMPC lipid bilayers. $^{13}C/^{13}C$ PDSD MAS exchange experiments on [$^{13}C_{\alpha}$,^{15}N-Leu] EmrE in the native state at a mixing time of 500 ms. Due to the dilute ^{13}C labeling of EmrE, the PDSD experiment serves as a ZZ-exchange experiment.[34] The lack of cross-peaks at −22 °C is indicative that the large-scale conformational exchange has been quenched and the cross-peaks observed at 9 °C are not due to magnetization exchange..

quantified at mixing times ranging from 0.1 and 1.5 s and subsequently fit to obtain an exchange rate (k_{ex}) of ∼1.9 s^{-1} (SI Figure 9). Lastly, a control experiment was carried out at −22 °C that displayed no off-diagonal peaks in the spectrum, and was confirmation that the cross-peaks detected at 9 °C were not due to magnetization transfer (Figure 6). Taken together, the dynamics data in three different membrane environments with residues throughout the protein confirmed the plasticity of the native EmrE structure relative to the TPP^+ bound form on the millisecond time scale.

Arrhenius Plot of Temperature-Dependent Conformational Exchange Rates. From the temperature-dependent exchange rates shown in SI Table I (solution NMR, oriented solid-state NMR, and MAS), we constructed an Arrhenius plot in order to calculate the activation energy barrier corresponding to the inward−outward conformational change (Figure 3C). The dynamics data acquired in bicelles and bilayers agrees with a single conversion event as evident from the quality of the Arrhenius fit (r^2 = 0.98). From this plot, we calculated an activation energy barrier for the inward−outward exchange of 28 ± 5 kcal/mol. To pursue the molecular origin of this activation energy, we focused on the interaction surface between the two EmrE monomers within the dimer. A model of EmrE was constructed from the TPP^+-bound Cα crystal coordinates[15] using REMO[53] and used to calculate a surface area of ∼1240 Å^2 between the two EmrE monomers within the dimer.[54] However, the entire surface area is not likely disrupted in the conformational change between inward-open and outward-open states. For example, the homologous protein, Hsmr, is stabilized by TM4−TM4 contacts between the two monomers.[55] Since this interface may not dramatically change during the conformational change, we subtracted the surface area constituting TM4 interhelical interactions (∼320 Å^2) from the total estimated dimer interface. Using this adjusted area of 920 Å^2 and an empirical value of ∼26.3 cal/mol free energy per 1 Å^2 of hydrophobic contact for membrane proteins,[56] we obtained a value of 24 kcal/mol, which was in good agreement with the energy barrier determined by our NMR experiments. While this calculation constitutes only an approximation due to the need for a high-resolution structure of native EmrE, these results support the conclusion that a significant portion of the total intermonomer surface area contact must be broken in order to switch from the outward-open to inward-open conformation. It is also important to note that in the alternating access model the broken intermolecular contacts are remade as

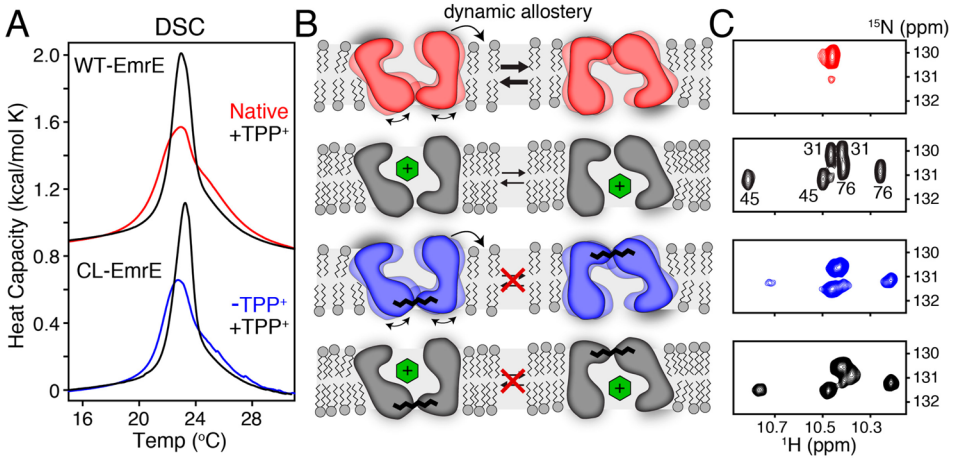

Figure 7. Dynamic allostery and the impact on the lipid bilayer phase transition. (A) DSC thermograms for wild-type and CL-EmrE in the absence and presence of TPP^+ in DMPC lipid bilayers at a lipid/monomer molar ratio of 100/1. Fitted parameters including the temperature, enthalpy, and half-height of the main phase transition are shown in SI Table II. No effect of TPP^+ alone was observed on the melting profile of DMPC bilayers (SI Figure 12). (B) Model representation of the large- and small-scale conformational rearrangements of EmrE that highlight the faster nanosecond−microsecond motions as the primary driving mechanism of reduced bilayer melting cooperativity. The small-scale transitions persist for both EmrE and CL-EmrE in the absence of substrate. (C) $^1H/^{15}N$ TROSY-HSQC spectra of the indole region of EmrE at 45 °C, which shows two populations for substrate-free CL-EmrE that supports halting of the millisecond time scale dynamics.

dx.doi.org/10.1021/ja503145x | J. Am. Chem. Soc. 2014, 136, 8072−8080

a consequence of the conformational change and thus the net free energy change is zero.

Effect of EmrE Dynamics on the Lipid Bilayer. On the basis of our NMR results that elucidated the plasticity of native EmrE, we anticipated that the inward−outward conformational dynamics might manifest an effect on the physical properties of the lipid bilayer. In order to test this hypothesis, we used DSC to probe the main phase transition (T_m), width of the transition ($\Delta T_{1/2}$), and melting enthalpy of the bilayer. These experiments were carried out in the presence and absence of TPP^+ at a 100/1 DMPC/EmrE molar ratio in hydrated liposomes under identical reconstitution conditions as those used for solution and solid-state NMR experiments. Interestingly, we observed a broader phase transition for native EmrE (4.0 ± 0.1 °C) relative to the TPP^+-bound form (2.0 ± 0.1 °C) (Figure 7A). In other words, native EmrE was able to decrease the bilayer melting cooperativity likely by reducing the packing between annular and bulk lipids (schematic depiction in Figure 7B).[57] In contrast, no major changes were found for either the main phase transition temperature or the melting enthalpy between native and TPP^+-bound EmrE (SI Table II). These results were intriguing given that we also observed small but significant differences in the solution NMR line widths for native EmrE (^{1}H: 24 ± 2 Hz) relative to the TPP^+-bound form (^{1}H: 21 ± 1 Hz). This NMR peak broadening suggested the presence of residual conformational dynamics on a faster time scale (nanosecond−microsecod) than those corresponding to the inward−outward millisecond time scale motion.

Was the major inward-open to outward-open conformational transition responsible for the broadening of the phase transition or were faster motions at play? To answer this question, we repeated DSC and solution NMR experiments using cross-linked EmrE dimers (CL-EmrE) with the goal of removing the inward−outward exchange. Previously, it was shown that a functional EmrE mutant (C39S, C41S, C95S, S107C) could be cross-linked using the heterobifunctional molecule N-(β-maleimidopropyloxy)succinimide ester (BMPS), which resulted in a stable, covalent linkage between the side chains of K22 and C107 in opposite monomers.[16] After optimizing this reaction to achieve nearly complete cross-linking (SI Figure 10A), we verified that the fused dimer binds TPP^+ with similar affinity as wild-type EmrE (K_d = 187 nM; SI Figure 10B).[16] Solution NMR experiments were then acquired using a sample of [U-^{15}N] CL-EmrE, which behaved similarly to the wild-type protein in the purification (i.e., no tendency to aggregate). However, unlike the wild-type native form, the ^{1}H/^{15}N TROSY-HSQC spectrum at 45 °C of substrate-free CL-EmrE showed the presence of peak doubling (Figure 7C), which was direct evidence that the inward−outward dynamics in the covalent dimer were halted. Interestingly, the DSC thermograms for substrate-free CL-EmrE in DMPC vesicles exhibited a profile resembling that of the wild-type native transporter (Figure 7A). In other words, the inward−outward large-scale conformational change was not the primary source of the phase transition broadening; instead, the presence of residual conformational plasticity within each of the inward and outward facing structural ensembles of native EmrE was likely responsible for the bilayer perturbations. Only after addition of TPP^+ to CL-EmrE did the $\Delta T_{1/2}$ and NMR peak intensities agree with those of substrate-bound wild-type EmrE (Figure 7). Given the faster time scale of lipid motions relative to the protein dimer stemming from the ∼35-fold mass difference, these results are consistent with the conclusion that small-scale conformational fluctuations within native EmrE (nanosecond−microsecond time scale) have a more pronounced effect on bilayer packing than the large-scale inward-open to outward-open conformational rearrangement (millisecond time scale).

CONCLUSION

The ability to characterize the structural dynamics of efflux pumps is necessary in order to decipher the inner workings of the transport cycle. In this process, drug transport needs to be tightly coupled with the proton motive force.[58] Using a hybrid of NMR approaches, we probed the dynamics of native EmrE and found that the transporter undergoes rapid conformational switching at a rate of ∼300 s^{-1} at 37 °C and a pH of 6.9 (∼50-fold faster than TPP^+-bound EmrE). In other words, once the drug is released on the periplasmic side of the membrane, the native state can rapidly bind protons[60] and then convert to the inward facing side to begin a subsequent round of transport. Our findings also suggest a possible mechanism for how EmrE mutants are able to import polyamines as recently reported by Schuldiner and co-workers.[59] In this model, the millisecond inward-open to outward-open conformational motions of mutant EmrE may allow the transporter to have both periplasmic and cytoplasmic facing conformations necessary for export and import activities that could fulfill an evolutionary need stemming from environmental pressures in bacteria.

In addition to the outward-open to inward-open transition in the absence of drug, there are a number of key steps in the overall transport cycle that include (a) cytoplasmic proton release, (b) cytoplasmic drug binding, (c) conversion to the outward-open state, (d) periplasmic release of substrate, and (e) binding of protons in the periplasm.[12] Given that TPP^+ release occurs with an off-rate of ∼0.5 s^{-1} at pH = 6.9,[60] the apparent inward-open to outward-open interconversion rates for EmrE bound to TPP^+ of 4.9 s^{-1} (45 °C)[18] and 3.2 s^{-1} (this work, 37 °C) suggest that this step may also contribute to the overall turnover rate.[61] This emphasizes that the conformational change between periplasmic and cytoplasmic facing configurations in the absence of drug is not the rate-limiting step in the transport cycle of TPP^+. It is important to note that while TPP^+ has been a useful molecule for structural and binding studies,[13,15−18,60,62] it is not transported as efficiently as other substrates such as methyl viologen or ethidium.[63] Additional high-resolution studies are needed to determine inward-open to outward-open conformational rates in the presence of these substrates. Toward this objective, Morrison et al. has reported that the structure of the transported substrate can significantly affect the observed exchange rate.[61] Based on the findings of their work, it is possible that the exchange rate for more efficiently transported substrates such as methyl viologen and ethidium will be greater than that observed for TPP^+.

Large amplitude dynamics are needed for substrate transport in multidrug resistance efflux pumps where drugs are shuttled from the cytoplasmic to periplasmic side of the membrane. Our data support the conclusion that underlying faster time scale dynamics (nanosecond−microsecond) in the native state collectively *speed up* the rate of the outward-open to inward-open conformational change for the native form relative to that found with TPP^+. We propose that these dynamics enable native EmrE to cross the conformational energy barrier we calculated from our temperature-dependent measurements. This idea underscores the broader lipid bilayer phase transitions that were observed in the native state of wild-type and cross-

linked EmrE and implicates a role of residual conformational entropy[64,65] to overcome the enthalpy barrier for alternating between outward-open and inward-open states to achieve broad multidrug recognition and resistance. It is expected that this barrier is altered for drug-bound forms,[61] which would reflect differential packing within the hydrophobic binding pocket and the overall available free energy of EmrE. Taken together, our findings provide a clear example how substrate binding affects membrane protein dynamics that perturbs the physical properties of the lipid bilayer in an allosteric fashion.

■ ASSOCIATED CONTENT

Supporting Information

Additional figures of NMR spectra, line shape fitting, binding of TPP^+ to cross-linked EmrE, and a table with exchange rates. This material is available free of charge via the Internet at http://pubs.acs.org.

■ AUTHOR INFORMATION

Corresponding Author

traaseth@nyu.edu

Author Contributions

[†]These authors made an equal contribution.

Notes

The authors declare no competing financial interest.

■ ACKNOWLEDGMENTS

This work was supported by NIH Grant 5K22AI083745 and start-up funds from New York University; J.R.B. acknowledges support from a Margaret Strauss Kramer Fellowship. The NMR data collected at the New York Structural Biology Center was made possible by grants from NYSTAR, NIH (CO6RR015495, P41GM066354), the Keck Foundation, New York State Assembly, and the U.S. Department of Defense. We also thank Prof. Lara Mahal for sharing protein purification equipment, and Prof. Jin Montclare for use of the DSC instrument.

■ REFERENCES

(1) Fischbach, M. A.; Walsh, C. T. *Science* **2009**, *325*, 1089−1093.
(2) Neu, H. C. *Science* **1992**, *257*, 1064−1073.
(3) Walsh, C. *Nature* **2000**, *406*, 775−781.
(4) Piddock, L. J. *Nat. Rev. Microbiol.* **2006**, *4*, 629−636.
(5) Jardetzky, O. *Nature* **1966**, *211*, 969−970.
(6) Zheng, H.; Wisedchaisri, G.; Gonen, T. *Nature* **2013**, *497*, 647−651.
(7) Yan, N. *Trends Biochem. Sci.* **2013**, *38*, 151−159.
(8) Boudker, O.; Verdon, G. *Trends Pharmacol. Sci.* **2010**, *31*, 418−426.
(9) Lolkema, J. S.; Dobrowolski, A.; Slotboom, D. J. *J. Mol. Biol.* **2008**, *378*, 596−606.
(10) Bay, D. C.; Turner, R. J. *BMC Evol. Biol.* **2009**, *9*, 140.
(11) Schuldiner, S. *Biochim. Biophys. Acta* **2009**, *1794*, 748−762.
(12) Schuldiner, S. In *Membrane Transport Mechanism*; Kramer, R., Ziegler, C., Eds.; Springer: Berlin, 2014; Vol. Springer Series in Biophysics *17*, pp 233−248.
(13) Ubarretxena-Belandia, I.; Baldwin, J. M.; Schuldiner, S.; Tate, C. G. *EMBO J.* **2003**, *22*, 6175−6181.
(14) Tate, C. G.; Kunji, E. R.; Lebendiker, M.; Schuldiner, S. *EMBO J.* **2001**, *20*, 77−81.
(15) Chen, Y. J.; Pornillos, O.; Lieu, S.; Ma, C.; Chen, A. P.; Chang, G. *Proc. Natl. Acad. Sci. U.S.A.* **2007**, *104*, 18999−19004.
(16) Gayen, A.; Banigan, J. R.; Traaseth, N. J. *Angew. Chem., Int. Ed.* **2013**, *52*, 10321−10324.
(17) Lehner, I.; Basting, D.; Meyer, B.; Haase, W.; Manolikas, T.; Kaiser, C.; Karas, M.; Glaubitz, C. *J. Biol. Chem.* **2008**, *283*, 3281−3288.
(18) Morrison, E. A.; DeKoster, G. T.; Dutta, S.; Vafabakhsh, R.; Clarkson, M. W.; Bahl, A.; Kern, D.; Ha, T.; Henzler-Wildman, K. A. *Nature* **2012**, *481*, 45−50.
(19) Seppala, S.; Slusky, J. S.; Lloris-Garcera, P.; Rapp, M.; von Heijne, G. *Science* **2010**, *328*, 1698−1700.
(20) Yerushalmi, H.; Schuldiner, S. *J. Biol. Chem.* **2000**, *275*, 5264−5269.
(21) Ong, Y. S.; Lakatos, A.; Becker-Baldus, J.; Pos, K. M.; Glaubitz, C. *J. Am. Chem. Soc.* **2013**, *135*, 15754−15762.
(22) Basting, D.; Lorch, M.; Lehner, I.; Glaubitz, C. *FASEB J.* **2008**, *22*, 365−373.
(23) Korkhov, M. V.; Tate, C. G. *J. Mol. Biol.* **2008**, *377*, 1094−1103.
(24) Delaglio, F.; Grzesiek, S.; Vuister, G. W.; Zhu, G.; Pfeifer, J.; Bax, A. *J. Biomol. NMR* **1995**, *6*, 277−293.
(25) Rogers, M. T.; Woodbrey, J. C. *J. Phys. Chem.* **1962**, *66*, 540−546.
(26) Banigan, J. R.; Gayen, A.; Traaseth, N. J. *J. Biomol. NMR* **2013**, *55*, 391−399.
(27) Hediger, S.; Meier, B. H.; Ernst, R. R. *Chem. Phys. Lett.* **1995**, *240*, 449−456.
(28) Szeverenyi, N. M.; Sullivan, M. J.; Maciel, G. E. *J. Magn. Reson.* **1982**, *47*, 462−475.
(29) Ammann, C.; Meier, P.; Merbach, A. E. *J. Magn. Reson.* **1982**, *46*, 319−321.
(30) Bennett, A. E.; Rienstra, C. M.; Auger, M.; Lakshmi, K. V.; Griffin, R. G. *J. Chem. Phys.* **1995**, *103*, 6951−6958.
(31) Cavanagh, J.; Fairbrother, W. J.; Palmer III, A. G.; Skelton, N. J. *Protein NMR Spectroscopy: Principles and Practice*, 2nd ed.; Elsevier Academic Press: Amsterdam, 2007.
(32) Morcombe, C. R.; Zilm, K. W. *J. Magn. Reson.* **2003**, *162*, 479−486.
(33) Fung, B. M.; Khitrin, A. K.; Ermolaev, K. *J. Magn. Reson.* **2000**, *142*, 97−101.
(34) Montelione, G. T.; Wagner, G. *J. Am. Chem. Soc.* **1989**, *111*, 3096−3098.
(35) deAzevedo, E. R.; Bonagamba, T. J.; Schmidt-Rohr, K. *J. Magn. Reson.* **2000**, *142*, 86−96.
(36) deAzevedo, E. R.; Tozoni, J. R.; Schmidt-Rohr, K.; Bonagamba, T. J. *J. Chem. Phys.* **2005**, *122*, 154506.
(37) Tugarinov, V.; Kay, L. E. *ChemBioChem* **2005**, *6*, 1567−1577.
(38) Sharma, M.; Yi, M.; Dong, H.; Qin, H.; Peterson, E.; Busath, D. D.; Zhou, H. X.; Cross, T. A. *Science* **2010**, *330*, 509−512.
(39) Page, R. C.; Kim, S.; Cross, T. A. *Structure* **2008**, *16*, 787−797.
(40) Traaseth, N. J.; Shi, L.; Verardi, R.; Mullen, D. G.; Barany, G.; Veglia, G. *Proc. Natl. Acad. Sci. U.S.A.* **2009**, *106*, 10165−10170.
(41) Traaseth, N. J.; Verardi, R.; Torgersen, K. D.; Karim, C. B.; Thomas, D. D.; Veglia, G. *Proc. Natl. Acad. Sci. U.S.A.* **2007**, *104*, 14676−14681.
(42) De Angelis, A. A.; Howell, S. C.; Nevzorov, A. A.; Opella, S. J. *J. Am. Chem. Soc.* **2006**, *128*, 12256−12267.
(43) Durr, U. H.; Yamamoto, K.; Im, S. C.; Waskell, L.; Ramamoorthy, A. *J. Am. Chem. Soc.* **2007**, *129*, 6670−6671.
(44) Knox, R. W.; Lu, G. J.; Opella, S. J.; Nevzorov, A. A. *J. Am. Chem. Soc.* **2010**, *132*, 8255−8257.
(45) Nevzorov, A. A.; DeAngelis, A. A.; Park, S. H.; Opella, S. J. In *NMR Spectroscopy of Biological Solids*; Ramamoorthy, A., Ed.; Marcel Dekker: New York, 2005; pp 177−190.
(46) Wu, C. H.; Ramamoorthy, A.; Opella, S. J. *J. Magn. Reson.* **1994**, *109*, 270−272.
(47) Gopinath, T.; Veglia, G. *J. Am. Chem. Soc.* **2009**, *131*, 5754−5756.
(48) Ramamoorthy, A.; Wei, Y.; Dong-Kuk, L. *Annu. Rev. NMR Spectrosc.* **2004**, *52*, 1−52.
(49) Traaseth, N. J.; Gopinath, T.; Veglia, G. *J. Phys. Chem. B* **2010**, *114*, 13872−13880.

(50) Fleishman, S. J.; Harrington, S. E.; Enosh, A.; Halperin, D.; Tate, C. G.; Ben-Tal, N. *J. Mol. Biol.* **2006**, *364*, 54−67.
(51) Agarwal, V.; Fink, U.; Schuldiner, S.; Reif, B. *Biochim. Biophys. Acta* **2007**, *1768*, 3036−3043.
(52) Hong, M.; Jakes, K. *J. Biomol. NMR* **1999**, *14*, 71−74.
(53) Li, Y. Q.; Zhang, Y. *Proteins* **2009**, *76*, 665−674.
(54) Krissinel, E.; Henrick, K. *J. Mol. Biol.* **2007**, *372*, 774−797.
(55) Poulsen, B. E.; Cunningham, F.; Lee, K. K.; Deber, C. M. *J. Bacteriol.* **2011**, *193*, 5929−5935.
(56) Faham, S.; Yang, D.; Bare, E.; Yohannan, S.; Whitelegge, J. P.; Bowie, J. U. *J. Mol. Biol.* **2004**, *335*, 297−305.
(57) Zhang, Y. P.; Lewis, R. N. A. H.; Hodges, R. S.; Mcelhaney, R. N. *Biochemistry* **1992**, *31*, 11579−11588.
(58) Soskine, M.; Adam, Y.; Schuldiner, S. *J. Biol. Chem.* **2004**, *279*, 9951−9955.
(59) Brill, S.; Falk, O. S.; Schuldiner, S. *Proc. Natl. Acad. Sci. U.S.A.* **2012**, *109*, 16894−16899.
(60) Adam, Y.; Tayer, N.; Rotem, D.; Schreiber, G.; Schuldiner, S. *Proc. Natl. Acad. Sci. U.S.A.* **2007**, *104*, 17989−17994.
(61) Morrison, E. A.; Henzler-Wildman, K. A. *J. Biol. Chem.* **2014**, *289*, 6825−6836.
(62) Amadi, S. T.; Koteiche, H. A.; Mishra, S.; McHaourab, H. S. *J. Biol. Chem.* **2010**, *285*, 26710−26718.
(63) Yerushalmi, H.; Lebendiker, M.; Schuldiner, S. *J. Biol. Chem.* **1995**, *270*, 6856−6863.
(64) Frederick, K. K.; Marlow, M. S.; Valentine, K. G.; Wand, A. J. *Nature* **2007**, *448*, 325−329.
(65) Tzeng, S. R.; Kalodimos, C. G. *Nature* **2012**, *488*, 236−240.